

ADVANCED PHASE-BASED SEGMENTATION OF MULTIPLE CELLS FROM BRIGHTFIELD MICROSCOPY IMAGES

Rehan Ali¹, Mark Gooding PhD², Martin Christlieb PhD³, Michael Brady FRS FEng¹

¹ Wolfson Medical Vision Labs, Dept of Engineering Science, University of Oxford

² Nuffield Dept of Obstetrics and Gynaecology, University of Oxford

³ Gray Cancer Institute, University of Oxford

ABSTRACT

Segmenting transparent phase objects, such as biological cells from brightfield microscope images, is a difficult problem due to the lack of observable intensity contrast and noise. Previous image analysis solutions have used excessive defocusing or physical models to obtain the underlying phase properties. Here, an improved cell boundary detection algorithm is proposed to accurately segment multiple cells within the level set framework. This uses a novel speed term based on local phase and local orientation derived from the monogenic signal, which renders the algorithm invariant to intensity, making it ideal for these images. The new method can robustly handle noise and local minima, and distinguish touching cells. Validation is shown against manual expert segmentations.

Index Terms— Biomedical image processing, Microscopy, Image segmentation

1. INTRODUCTION

Cell biologists acquiring microscopic single cell images often combine fluorescence microscopy, for functional imaging, along with brightfield microscopy to acquire anatomical information with which to localise the fluorescence signals (a process analogous to PET/CT for whole body imaging). However brightfield cell images are difficult to analyse with conventional intensity-based methods due to the lack of intensity contrast between the cells and background. The presence of noise, uneven background intensities from inhomogenous light sources, and artefacts on the lens can complicate image analysis further. Defocusing improves the contrast, but at the expense of resolution due to blurring by the point-spread function.

There has been renewed interest in brightfield image cell segmentation in recent literature. Texture differences offer a potential method of discriminating cells from background in in-focus images. Korzynska *et al* [1] use information from both second moment statistics for quantifying texture and a Prewitt edge detector, however the parameterisation of their method is initialisation-sensitive. Texture-based methods can

also be confused by lens artefacts such as the dark spots in Figure 2a. Tscherepanow *et al* [2] recognise the requirement for additional information when segmenting complex shapes, and introduce an extra DIC (Differential Interference Contrast) microscope image in their active snakes method. Our previous work [3] requires multiple defocused images to assist the initialisation of a level set, and extracts additional information using local phase, an intensity-invariant feature detector computed using the monogenic signal [4]. An alternative approach uses models of light propagation to recover the underlying physical phase, by solving the Transport of Intensity (TIE) equation [5]

$$-k\partial_z I(x, y) = \nabla_{\perp} \cdot [I(x, y)\nabla_{\perp}\Theta(x, y)] \quad (1)$$

where $I(x, y)$ is the image intensity, ∇_{\perp} is the gradient operator orthogonal to the image x-y plane, and $\Theta(x, y)$ is the physical phase. The TIE is commonly solved using the Fast Fourier Transform as described in [6], and in theory yields promising images with higher contrast. Applications of this approach to brightfield cell images have been based primarily on thresholding [7] or simple shape fitting [8]. However several reports [9] [10] and our own work show that recovering phase using this method under sub-optimal conditions can create strong low-frequency artefacts. These obscure the cell signal, even after applying periodic boundary conditions and low-frequency filtering, making consistent cell edge detection difficult.

Our new approach extends [3] in several ways. First, it

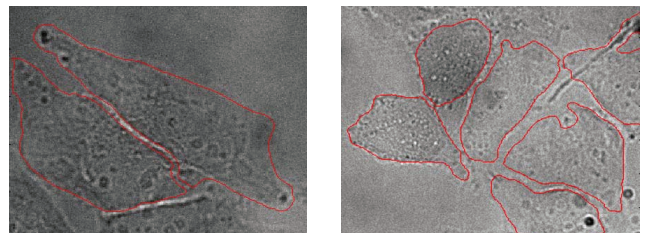


Fig. 1. Two segmentation results (red contours) of HeLa cells observed by brightfield microscopy, using our method.

simplifies the input requirements to two brightfield images, one less than the TIE-based approaches. More efficient use is made of the information derived from the monogenic signal, enabling the computation of an improved speed term which is able to escape from local minima. The level set framework is used to segment multiple objects, and the algorithm is able to separate and keep apart touching cells. The new method is not only more accurate, but also more robust to lens artefacts and background inhomogeneities.

Figure 1 shows some typical segmentation results obtained by our method. The next section outlines the methods used, and Section 3 presents the results and validations. A discussion of the method and its potential applications is given in Section 4.

2. METHOD

2.1. Image Acquisition

Transillumination brightfield images were acquired for HeLa immortal cervical cancer cells using an inverted Nikon Eclipse TE2000E epifluorescence microscope at 40x magnification, illuminated with a mercury arc 100W lamp without any frequency filters. Two images were acquired symmetrically just above and below the focal plane ($\Delta z = \pm 5\mu m$). An in-focus image ($\Delta z = 0$) was also acquired for reference.

2.2. Initialisation

A derivative image across $\Delta z = 0$ is created from the out-of-focus images (Figure 2B), similar to the first step when solving the TIE. This normalises the background and removes any lens-based artefacts that will be present in both images (as they will be invariant to defocusing).

$$\frac{\partial I(x, y, 0)}{\partial z} \approx I(x, y, +\Delta z) - I(x, y, -\Delta z) \quad (2)$$

A common technique in 1D feature detection is the use of band-pass quadrature filters, derived using the analytic signal. These are applied to windowed signals in order to extract a property known as local phase, which is sensitive to the presence of a feature. The monogenic signal [4] is a multi-dimensional generalisation of the analytic signal, and we use it with a quadrature triple filter set to compute local phase (Figures 2C) and local orientation (Figures 2D). The filters are based on a filter family developed by Mellor *et al* [11]:

$$f(r) = \frac{A}{r^{\alpha+\beta}} - \frac{B}{r^{\alpha-\beta}} \quad (3)$$

where r is the filter radius, A, B are arbitrary constants, and $\alpha = 0.25$ and $\beta = 0.025$. This creates a lowpass filter, which is unusual when computing the monogenic signal, however it allows us to isolate large-scale features in our images. Unwanted background features in the resultant local

phase map are removed by masking them with a thresholded variance map of the derivative image, and the corrected local phase map is thresholded to generate an estimation of the cell regions. Each region is uniquely labelled using connected components to generate an $(n + 1)$ -class initialisation map (describing n identifiable cell regions plus background). A manual step is then performed where the user clicks once in each cell (thus defining m cells, where $m \geq n$).

2.3. Splitting Touching Cells

The initialisation process can yield regions which contain multiple touching cells. These are separated by performing region growing on the labelled initialisation map from each of the user-defined seed points to give $m + 1$ classes. This step, coupled with our level set which prevents region merging (see next section), ensures that each cell is separately segmented, and the level set is able to compensate for any incorrectly defined boundaries between neighbouring cells.

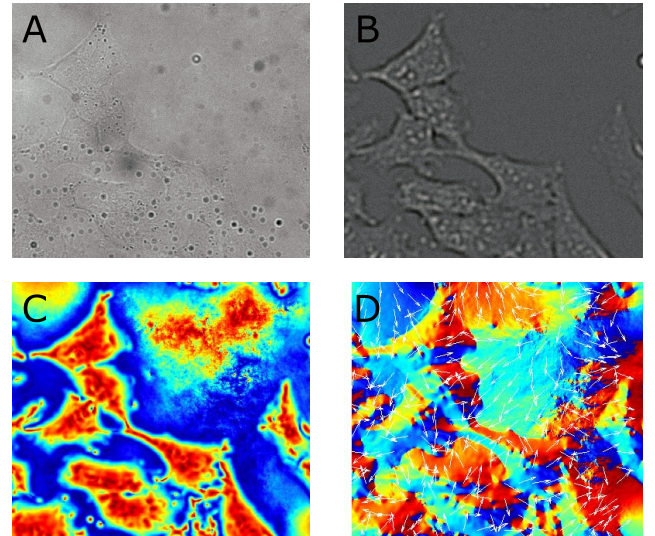


Fig. 2. (A) In-focus image of a cluster of touching HeLa cells, (B) derivative image, (C) local phase map, (D) local orientation map (with directional arrows superimposed).

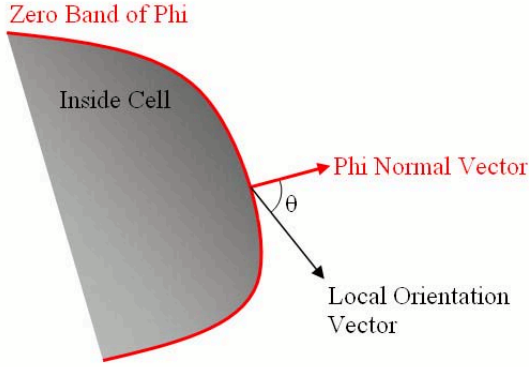
2.4. Level Set Evolution

A narrowband multi-region level set implementation by Gooding *et al* [12] is used. A signed distance ϕ is generated from the initialisation map, and the level set PDE below is solved to convergence:

$$\frac{\partial \phi}{\partial t} + F |\nabla \phi| = 0 \quad (4)$$

where the speed term F is given by

$$F = \alpha F_{phase} + \beta F_{orientation} + \gamma F_{smooth} \quad (5)$$



If $\cos(\theta) < 0$	If $\cos(\theta) = 0$	If $\cos(\theta) > 0$
Contracting force	No effect	Expansion force

Fig. 3. The local orientation force used to drive the level set function.

F_{phase} is a PDF-based region term [12] computed over the local phase map. A local window PDF W is sampled at each point on the zero level set, and compared to the PDFs for the current cell class j and the neighbouring (cell or background) class i . The region term compares these distributions:

$$F_{phase} = \frac{pdfv(W) \cdot pdfv(i)}{\|pdfv(i)\|} - \max_{j \neq i} \left(\frac{pdfv(W) \cdot pdfv(j)}{\|pdfv(j)\|} \right) \quad (6)$$

where $pdfv(\cdot)$ is the vector form of the PDF, with dimension equal to the maximum number of intensity values (255).

$F_{orientation}$ is an orientation specific term. Local orientation is used to guide the level set evolution, by comparing it at each iteration to the direction of $\nabla(\phi = 0)$:

$$F_{orientation} = \cos(\theta_{\nabla\phi} - \theta_{LO}) \quad (7)$$

where $\theta_{\nabla\phi}$ is the angle of the normal vector of ϕ , and θ_{LO} is the local orientation angle. Where the two are in agreement, ϕ experiences a positive expansion force, whilst if the two are opposing then ϕ will experience a negative force (Figure 3).

F_{smooth} is a regularising term using the curvature of ϕ , and α, β, γ are weighting terms set to 1, 0.5 and 1 respectively (the algorithm is insensitive to small changes in these values). Finally the level set algorithm also contains an overriding repulsion term which sets $F = -1$ if two distinct regions are about to touch, to prevent region merging.

2.5. Validation

The results are compared against manual ground truths by expert cell biologists, and also against Lysotracker fluorescence images. Where the brightfield and fluorescence images are misaligned (due to specimen container shift within the microscope), they are realigned using mutual information rigid

registration [13] between the fluorescence image and the local phase map of the brightfield image.

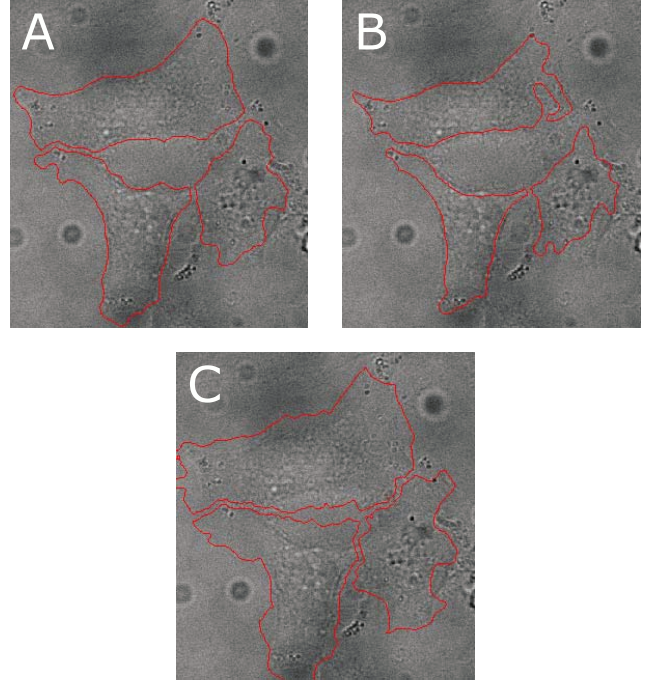


Fig. 4. (A) Segmentation results (red contours) using local phase and local orientation speed terms ($\alpha = 1, \beta = 0.5$), (B) using local phase alone ($\alpha = 1, \beta = 0$), and (C) using the local orientation term alone ($\alpha = 0, \beta = 0.5$).

3. RESULTS

Figure 4 shows how our speed term performs without the local phase or local orientation term. The local orientation term provides a strong driving force which compensates for regions where local phase information is weaker, and thus allows the level set to evolve quicker and escape from local minima such as the concavity in the corner of the top cell. However the local phase term is important for bounding the contour to the cell regions, and omitting this results in oversegmentation.

Figure 5 shows a segmentation result on a noisy image using the speed term in Equation 5. The results can be seen to correlate well with the cellular regions in the fluorescence image. There are several touching cells in the image, however the level set repulsion term successfully keeps them apart.

The method was evaluated against manual segmentations provided by three expert cell biologists. Using a sample of 134 cells, our algorithm correctly classified 83% of true cell pixels ($\pm 7\%$). This improves upon our previous method [3]. More importantly however, the new method is more robust against noise, and is able to work on cell images which our earlier method fails on.

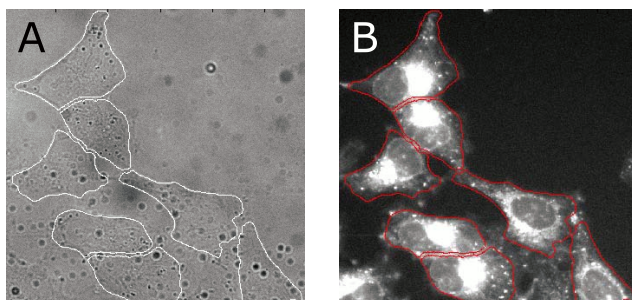


Fig. 5. Segmentation result overlaid on (A) the brightfield image in Figure 2A (white contour), and (B) a LysoTracker (Invitrogen Corporation TM) fluorescence image (red contour).

4. DISCUSSION

Despite the work done to date on brightfield microscopy image analysis, there is considerable scope for improvement by using recent developments from the broader medical vision field. The monogenic signal is such an example, as it has been successfully used in similar problems (e.g. breast mammogram feature detection [14]) where there is weak feature information in the intensity data. We use it to extract local phase and local orientation from our brightfield images, enabling a robust speed function to be used within a multi-region level set approach.

Our method has been shown to segment cells from challenging image data, and is sufficiently accurate to be able to quantify intracellular fluorescence and cell structure. We plan to use it as a tool for investigating the uptake/efflux pharmacokinetics of fluorescent derivatives of the hypoxia-selective PET tracer CuATSM in cancer cells [15], and for investigating the change in cancer cell morphology in response to tracer concentration under normoxic and hypoxic conditions. We also aim to develop the method further, by automating the algorithm's seeding and parameter selection to minimise user intervention, and using texture information to segment the regions currently being missed. Finally we have developed a user interface which we plan to make freely available to cell biologists for their research. Details of this interface can be found at www.sephace.com.

5. REFERENCES

[1] A Korzynska, W Stronjy, A Hoppe, D Wertheim, and P Hoser, "Segmentation of microscope images of living cells," *Patt Anal App*, vol. 10, no. 4, pp. 301–319, 2007.

[2] M Tscherepanow, N Nickels, and F Kummert, "Recognition of unstained live drosophila cells in microscope images," *IMVIP 2007*, pp. 169–176, 2007.

[3] R Ali, M Gooding, M Christlieb, and M Brady,

"Phase-based segmentation of cells from brightfield microscopy," *ISBI 2007*, pp. 57–60, 2007.

[4] M Felsberg and G Sommer, "The monogenic signal," *IEEE Trans Sig Proc*, vol. 49, no. 12, pp. 3136–3144, 2001.

[5] D Paganin and K Nugent, "Noninterferometric phase imaging with partially coherent light," *Phys Rev Lett*, vol. 80, no. 12, pp. 2586–2589, 1998.

[6] V Volkov, Y Zhu, and M De Graef, "A new symmetrized solution for phase retrieval using the transport of intensity equation," *Micron*, vol. 33, no. 5, pp. 411–416, 2002.

[7] C Curl, T Harris, P Harris, B Allman, C Bellair, A Stewart, and L Delbridge, "Quantitative phase microscopy: a new tool for measurement of cell culture growth and confluency in situ," *Eur J Physiol*, vol. 448, pp. 462–468, 2004.

[8] O Veselow, W Polak, R Ugenskiene, K Lebed, J Lekki, Z Stachura, and J Stychzen, "Development of the ifj single ion hit facility for cell irradiation," *Radiation Protection Dosimetry*, vol. 122, no. 1-4, pp. 316–319, 2006.

[9] L Allen and M Oxley, "Phase retrieval from series of images obtained by defocus variation," *Optics Comm*, vol. 199, pp. 65–75, 2001.

[10] M Bellegia, M Schofield, V Volkov, and Z Zhu, "On the transport of intensity technique for phase retrieval," *Ultramicroscopy*, vol. 102, no. 1, pp. 37–49, 2004.

[11] M Mellor and M Brady, "Phase mutual information as a similarity measure for registration," *Med Image Analysis*, vol. 9, no. 4, pp. 330–43, 2005.

[12] M Gooding, S Kennedy, and J Noble, "Volume segmentation and reconstruction from freehand 3d ultrasound data with application to ovarian follicle measurement," *Ultrasound Med Biol (in press)*, 2007.

[13] W Wells, P Viola, H Atsumi, S Nakajima, and R Kikinis, "Multi-modal volume registration by maximization of mutual information," *Med Im Anal*, vol. 1, no. 1, 1996.

[14] X Pan, M Brady, R Highnam, and J Declerck, *The Use of Multi-scale Monogenic Signal on Structure Orientation Identification and Segmentation (from Lecture Notes in Computer Science)*, Springer Berlin, 2006.

[15] S Pascu, P Waghorn, J Dilworth, M Christlieb, and J Warren, "Designing zn(ii) and cu(ii) derivatives as probes for in vitro fluorescence imaging," *Chem. Commun.*, pp. 4988–4997, 2007.